International Journal of Mass Spectrometry 277 (2008) 130–141

Contents lists available at ScienceDirect

International Journal of Mass Spectrometry

journal homepage: www.elsevier.com/locate/ijms

Low-energy electron attachment to chloroform ($CHCl_3$) molecules: A joint experimental and theoretical study

J. Kopyra[a], I. Szamrej[a], K. Graupner[b], L.M. Graham[b], T.A. Field[b], P. Sulzer[c], S. Denifl[c], T.D. Märk[c], P. Scheier[c], I.I. Fabrikant[d], M. Braun[e], M.-W. Ruf[e], H. Hotop[e,*]

[a] Chemistry Department, University of Podlasie, Siedlce, Poland
[b] Department of Physics and Astronomy, Queen's University Belfast, Belfast, BT7 1NN, UK
[c] Institut für Ionenphysik und Angewandte Physik, Universität Innsbruck, A - 6020 Innsbruck, Austria
[d] Department of Physics and Astronomy, University of Nebraska, Lincoln, NE 68588-0111, USA
[e] Fachbereich Physik, Technische Universität Kaiserslautern, D - 67653 Kaiserslautern, Germany

ARTICLE INFO

Article history:
Received 10 April 2008
Received in revised form 16 May 2008
Accepted 20 May 2008
Available online 27 May 2008

Keywords:
Electron attachment
Cross section
Branching ratio
R-matrix calculation
$CHCl_3$

ABSTRACT

Results from a joint experimental and theoretical study of electron attachment to chloroform ($CHCl_3$) molecules in the gas phase are reported. In an electron swarm study involving a pulsed Townsend technique with equal gas and electron temperatures, accurate attachment rate coefficients were determined over the temperature range 295–373 K; they show an Arrhenius-type rise with increasing temperature, corresponding to an activation energy of 0.11(1) eV. In a high resolution electron beam experiment involving two versions of the laser photoelectron attachment method, the relative cross section for Cl^- formation from $CHCl_3$ over the energy range 0.001–1.25 eV at the gas temperature $T_G = 300$ K was measured. It exhibits clear downward cusp structure at the threshold for excitation of one quantum of the vibrational symmetric deformation mode ν_3, indicating that this mode is active in the primary attachment process. With reference to our thermal attachment rate coefficient $k(T = 300\,K) = 3.9(2) \times 10^{-9}$ cm^3 s^{-1}, a new highly resolved absolute attachment cross section for $T_G = 300$ K was determined. This cross section is extended to higher energies by measurements, carried out with a pulsed electron beam apparatus which also provided new data for the distinctly weaker fragment anions HCl_2^- and CCl_2^-. The resulting total absolute cross section for anion formation is used to calculate the dependence of the attachment rate coefficient $k(T_e;T_G)$ on electron temperature T_e over the range 50–15000 K at the fixed gas temperature $T_G = 300$ K. In addition, we report the dependence of the relative cross section for Cl^- formation on gas temperature ($T_G = 310$–435 K). For comparison with the experimental data, R-matrix calculations have been carried out for the dominant anion channel Cl^-. The results recover the main experimental observations and predict the dependence of the DEA cross section on the initial vibrational level ν_3 and on the vibrational temperature. Our results are compared with those of previous electron beam and electron swarm experiments.

1. Introduction

Attachment of low-energy electrons to molecules is an important process in gaseous dielectrics and other environments including excimer lasers, discharges used for etching, and the earth's atmosphere [1–3]. Due to the high electron affinity of halogen atoms Y dissociative electron attachment (DEA) to halogen containing molecules XY (short notation Y^-/XY)

$$e^-(E) + XY \rightarrow XY^{-*}(\mathrm{TNI}) \rightarrow X + Y^- \quad (1)$$

may often occur with large cross sections $\sigma(E)$ down to zero electron energy E, thus efficiently producing halogen anions as well as halogen atoms or halogen containing radicals which are important precursors for further reactions [1–5]. Following its formation, the excited, temporary negative ion XY^{-*} (TNI) can either decay by autodetachment (corresponding to elastic or inelastic electron scattering) or it may dissociate, thereby forming stable negative ions Y^-. In special cases (such as SF_6 [5–8]) long-lived anions XY^- may be formed by fast intramolecular vibrational redistribution (IVR) in the initially formed TNI.

One point of special interest in studies of the DEA process is the relation between the resonance energy (vertical attachment energy VAE) and the size of the DEA cross section at its respective maximum as well as the variation of these quantities with chemical

* Corresponding author. Tel.: +49 631 2052328; fax: +49 631 2053906.
E-mail address: hotop@physik.uni-kl.de (H. Hotop).

1387-3806/$ – see front matter © 2008 Elsevier B.V. All rights reserved.
doi:10.1016/j.ijms.2008.05.026

substitution [9]. As an example we consider the methane derivatives CH_3Cl, CH_2Cl_2, $CHCl_3$, and CCl_4. The lowest TNI state of these molecules has $^2A_1$ symmetry; it is responsible for electron attachment to these molecules at low energies via the process ($q = 1$–4, $p + q = 4$):

$$e^- + CH_pCl_q \rightarrow CH_pCl_q{}^{-*}(^2A_1) \rightarrow CH_pCl_{q-1} + Cl^- \quad (2)$$

The VAE of these molecules was studied by ab initio calculations [10,11] and by electron transmission spectroscopy (ETS) [12–14]. For CCl_4 the $^2A_1$ anion state has a negative VAE (from −0.34 to −0.08 eV [10,11]), i.e., it is bound relative to the vibrationless neutral molecule in the equilibrium conformation; its presence close to zero energy induces a very large attachment cross section at low energies, resulting in a high thermal attachment rate coefficient of $k(300\,K) = 3.79(19) \times 10^{-7}\,cm^3\,s^{-1}$ [15]. Substituting Cl atoms with H atoms raises the VAE substantially to 0.42 eV for $CHCl_3$, 1.01 eV for CH_2Cl_2, and 3.45 eV for CH_3Cl [14] while the thermal (300 K) attachment rate coefficients for these three molecules, relative to those for CCl_4, drop strongly by about two, five, and more than eight orders of magnitude [16]. Note that the DEA reaction (2) is an exothermic process for CCl_4, $CHCl_3$, and CH_2Cl_2 since the electron affinity of Cl (3.6127 eV [17]) exceeds the respective dissociation energy ($D^0_{298K} = 3.07, 3.22(2), 3.50(3)$ eV) for these three molecules [18]; for CH_3Cl ($D^0_{298K} = 3.63$ (2) eV [18]) reaction (2) is slightly endothermic.

In essence, the strong variation of the respective rate coefficients reflects the fact that electron attachment to molecules in the vibrational ground state at low electron energies is efficient only if the anion potential surface crosses that of the neutral near the equilibrium distance of the reaction coordinate. When the anion curve is raised to higher energies by increasing the VAE, its crossing point with the neutral curve is raised to larger distances and the Franck–Condon factor for attachment of near-zero energy electrons to molecules in the vibrational ground state decreases exponentially. In these cases, attachment to vibrationally excited molecules will exhibit strongly enhanced attachment cross sections at low electron energies [1,4,5,19–21]. Correspondingly, the vibrationally averaged cross section and the rate coefficient will show an Arrhenius-type rise with increasing vibrational temperature [1,19–24].

In this paper we concentrate on DEA to the molecule chloroform (trichloromethane $CHCl_3$). It possesses an electric dipole moment of 1.04 D = 0.41 a.u. [18] and a dipole polarizability of $64a_0^3$ (a_0 = Bohr radius = 52.9177 pm) [18], leading to a substantial long-range attraction for the electron. Electron collisions with $CHCl_3$ at low energies are strongly influenced by the $^2A_1$ resonance (VAE = 0.42 eV [14]) and by the doubly degenerate ^2E resonance (VAE = 1.76 eV [14]) which both arise from the three C–Cl σ* orbitals. These two resonances show up in both scattering [12,14] and DEA cross sections (see below). The predominant channel in DEA to $CHCl_3$ at low energies is Cl^- formation according to the reaction

$$e^- + CHCl_3 \rightarrow CHCl_3{}^{-*}(^2A_1) \rightarrow CHCl_2 + Cl^- + Q \quad (3)$$

with an exothermicity of $Q = 0.39(2)$ eV.

Low-energy electron attachment to $CHCl_3$ has been studied quite extensively, both by electron swarm [1,16,22,23,25–38] and by electron beam methods [9,39–46]. The swarm experiments yielded *thermal* attachment rate coefficients (i.e., equal electron temperature T_e and gas temperature T_G) at temperatures close to $T = 300$ K that scatter over the range $(1.3–5.0) \times 10^{-9}\,cm^3\,s^{-1}$. With rising temperature, the thermal rate coefficients were found to increase with an Arrhenius-type behaviour $k(T) = A\exp(-E_a/(k_BT))$ (k_B = Boltzmann constant), yielding activation energies E_a around 0.1 eV. Three different methods were applied to measure the dependence of the rate coefficients $k(T_e;T_G)$ on electron temperature for fixed gas temperature. Blaunstein and Christophorou [26] used a drift tube method to vary the mean electron energy $\langle E\rangle$ and found a maximum of about $2 \times 10^{-8}\,cm^3\,s^{-1}$ at $\langle E\rangle = 0.35$ eV ($T_G = 300$ K). Shimamori et al. [35] applied the microwave pulse radiolysis with microwave heating (MWPR-MH) method and reported results over the range from $T_e = T_G$ to $T_e \approx 12{,}000$ K ($\langle E\rangle = 1.5$ eV) at $T_G = 300$ K [23,35], 450 K and 600 K [23]. At $T_G = 300$ K, they found a maximum at $\langle E\rangle = 0.33$ eV [35] in agreement with the earlier work [26], but the respective absolute values and the shapes of the energy dependences are different. At $T_G = 450$ K, the rate coefficients at the lower T_e were found to rise strongly whereas the values near the maximum and above remained nearly the same [23]. At $T_G = 600$ K, the rate coefficients were observed to decrease slowly with rising $\langle E\rangle$ from a maximum of almost $3 \times 10^{-8}\,cm^3\,s^{-1}$ [23]. Spaněl et al. [36,38] used a flowing afterglow Langmuir probe (FALP) apparatus to study either (using helium as carrier gas) thermal ($T_e = T_G$) attachment or (with argon carrier gas) attachment occurring at $T_e > T_G = 300$ K with electron temperatures up to 4000 K (for details of the latter approach see [47]). Their rate coefficients showed a rise with increasing T_e similar to that observed in [23,35], but at higher absolute values.

DEA cross sections for anion formation from $CHCl_3$ have been measured in electron beam experiments at resolutions of (0.05–0.5) eV [9,39–46]. At energies below about 1 eV (only formation of Cl^-), the attachment spectra either showed a single rather broad peak [41,42] or a combination of a resolution-limited peak close to 0 eV and a broader peak with a maximum in the range (0.2–0.3) eV [9,40,43-46]. The near-zero energy peak was found to depend strongly on gas temperature, also indicating activation energies around 0.1 eV [44,45] while the peak at the higher energy appeared to be almost independent of gas temperature [45]. In an experiment carried out at a gas temperature $T_G \approx 338$ K, Aflatooni and Burrow [9] determined the absolute total attachment cross section at the maximum of this peak (observed at 0.27 eV [9,42]) as $9.6 \times 10^{-20}\,m^2$ with a quoted uncertainty of ±10%.

At energies below 3 eV, the anions HCl_2^- and CCl_2^- are weakly produced in addition to Cl^- [39,42] with broad, nearly Gaussian-shaped bands peaking at 1.6(1) and 1.45(10) eV, respectively [42]. Their energy-integrated intensities were determined as 0.2% and 0.07% (relative to that for Cl^- formation) [42] whereas in [39] the 'true relative peak heights' of these two bands are listed as 1:3. These processes occur through the higher-lying, doubly degenerate ^2E resonance. In recent DEA work on $CHCl_3$, Denifl et al. [46] reported attachment spectra for several additional very weak anion channels, namely CCl^-, Cl_2^-, $CHCl^-$, $CHCl_2^-$, CH^-, C^-, and H^-. Their spectra for Cl^-, HCl_2^-, and CCl_2^- showed maxima at 0.3, 1.71, and 1.56 eV and relative peak intensities of 100, 0.09, and 0.86, respectively.

An interesting detail of the attachment dynamics at very low electron energies was provided by an investigation of Rydberg electron transfer (RET) to $CHCl_3$ molecules, involving highly excited $K^{**}(nl)$ atoms for principal quantum numbers for $n = 10$ and $n = 40$ [48]. Measurements of the velocity and angular distributions of the product positive (K^+) and negative ions (Cl^-) revealed that the transient negative ions $CHCl_3{}^{-*}$ formed in the RET process undergo very rapid dissociation. This finding is not compatible with models of the DEA process involving $CHCl_3$ [36] which assume formation of a complex and randomization of rovibrational energy by IVR prior to dissociation.

For a detailed understanding of the DEA process, attachment cross sections should be measured over a range of gas temperatures with a sufficiently low-energy width to exhibit the true threshold behaviour of the cross section near zero energy. In the present work, we combine the results from four experiments to determine

a highly resolved absolute cross section for anion formation from $CHCl_3$ over the energy range 0–3.3 eV. Using an improved electron swarm apparatus, we redetermine the thermal attachment rate coefficient for $CHCl_3$ at an uncertainty of about 5% over the temperature range 295–373 K. Using two variants of the laser photoelectron attachment (LPA) method with an energy resolution of about 3 meV, we measure the relative cross section for formation of the dominant anion Cl^- over the energy range 0.001–1.25 eV at the well-defined gas temperature T_G = 300 K; with reference to the thermal rate coefficient at T = 300 K (3.9×10^{-9} cm^3 s^{-1}), the absolute scale of this DEA cross section is calibrated. In a medium resolution experiment involving a pulsed electron beam from a trochoidal electron monochromator and a time-of-flight mass spectrometer, we measure the relative cross sections for the anions Cl^-, HCl_2^-, and CCl_2^- at T_G = 300 K which are combined with the LPA results to establish absolute cross sections for these three anions over the range 0–3.3 eV. Finally, an electron beam apparatus, involving a hemispherical electron monochromator and a temperature-variable target beam source, is used to measure the dependence of the relative cross section for Cl^- formation on gas temperature over the range T_G = 310–435 K. In Section 2, we briefly describe the experimental setups and methods. In Section 3, we provide the essentials of the R-matrix calculations. In Section 4, we report the experimental results and compare them with previous experimental work and with the results of the R-matrix calculations. In Section 5, we conclude with a brief summary.

2. Experimental methods

2.1. Electron swarm experiment (Siedlce)

A pulsed Townsend (PT) technique [49,50] for studying electron attachment processes has been applied. The experimental procedure has been described in detail previously [51]. The apparatus consists of a reaction chamber, a 5 ns Nd:YAG frequency quadrupled laser (266 nm), a preamplifier, a fast oscilloscope and a power supply system. In the reaction chamber the two parallel electrodes separated by a distance d = 1.5 cm are stainless steel disks with a diameter of 6 cm. In our version of the PT technique a swarm of electrons is produced photoelectrically at the cathode using the pulsed laser. Carbon dioxide is used as a buffer gas which quickly thermalizes the electron swarm [52]. The electrons move towards the collecting electrode under the influence of a uniform electric field F. Traversing electrons induce a change of the anode potential which increases linearly as electrons move to the collecting electrode in the pure buffer gas. In the mixture of electron acceptor and buffer gas the electrons are captured by the attaching gas, and the increase in the potential is no longer linear. The current output signal is amplified by a preamplifier, registered on an oscilloscope and stored in a computer memory.

This technique allows separate measurements of the drift velocity W and of the thermal electron attachment rate coefficient $k(T)$. The drift velocity, at the particular F/N value (N = total density of the mixture), can be easily obtained from $W = d/t_0$, where t_0 is the electron swarm transit time which corresponds to the maximum of the current profile. The thermal electron attachment rate coefficient is determined from the shape of the pulse (as a function of the time).

The electron acceptor gas was introduced into the reaction chamber in an excess of carbon dioxide. CO_2 was provided by Fluka Co. with a stated purity of 99.998% and was used as delivered. The $CHCl_3$ sample (Chempur Co.) was of research grade purity (98.5% with 0.6–1% ethanol as stabilizer), and it was additionally purified by the freeze-pump-thaw technique before introduction into the reaction chamber. The applied pressure of the electron acceptor gas depends on its efficiency in attaching electrons and is chosen to yield an attachment rate of approximately 10^5 s^{-1}. For $CHCl_3$ we chose a partial pressure of 0.003–0.004 Torr. The total pressures of the gas mixtures were in the range 100–130 Torr.

2.2. TEM-TOF experiment (Belfast)

The DEA experiments at Belfast used a trochoidal electron monochromator (TEM) in combination with a time-of-flight (TOF) mass spectrometer. The apparatus has been described before in some detail [53], and only the essentials are summarized here. The electron beam path is immersed in a parallel guiding magnetic field of 0.008 T. A deflection plate in the beam-monitoring Faraday cup moves the electrons off-axis and thus prevents return of the electrons to the interaction region. The electron energy was set by floating the electron gun potentials relative to the interaction region. A plate near the filament is pulsed to send short (duration about 1 μs) pulses of electrons through the interaction region. A repeller plate is pulsed to push the product anions from the source region into the acceleration region of the TOF mass spectrometer after all the electrons have left the interaction region. The anions are further accelerated in the acceleration region before they pass through a field-free drift region and strike the multichannel plate detector. The repetition rate of this pulse scheme is 12 kHz. The apparatus is operated under conditions where at most one ion is detected per ten cycles to minimize any paralysis of the detector due to the arrival of two ions at the same time. The electron energy resolution (FWHM) was estimated from the width of the apparent SF_6^- yield due to electron attachment to SF_6 at near-zero energies and amounted to 0.25–0.37 eV.

The experiment was carried out at room temperature (T_G = 300 K). Liquid $CHCl_3$ with a stated purity of 99.8 % was provided by J.T. Baker Ltd. with a small quantity of ethanol (0.5–1.0%) added as a stabilizer. This sample was used without further purification. Gas dissolved in the liquid was removed with a number of freeze thaw cycles. The ethanol stabilizer forms no anions that could affect the results and in all cases the negative ions observed had the expected ratios of different masses due to ^{35}Cl and ^{37}Cl isotopes.

2.3. HEM-QMS experiment (Innsbruck)

For the present DEA experiments in Innsbruck a crossed electron/neutral beam apparatus is utilized. A more detailed description of the setup can be found in [54]. Briefly, a neutral beam of chloroform molecules intersects at right angle with a monochromatized electron beam generated by a hemispherical electron monochromator (HEM). Chloroform was purchased from Sigma-Aldrich and has a stated purity of 99% (with 0.5–1% ethanol as stabilizer). The electrons are produced by a hairpin filament and are accelerated with a lens system into a hemispherical electrostatic field analyzer (pass energy about 1.5 eV), where the electron energy distribution for the present experiment is reduced to a value of about 80 meV. This resolution is chosen in favour of a higher detection sensitivity of the apparatus whereas better energy resolutions up to the optimum value of 35 meV result in too low electron and ion currents. The monochromatized electrons are accelerated with a second lens system to the desired energy and focused into the collision chamber.

The chloroform gas is introduced via a curved stainless steel tube (inner diameter 1.6 mm), connected to an external gas inlet system and directly reaching into the collision chamber of the HEM to a point located about 1 cm from the electron beam crossing point. Both the gas inlet tube and the HEM are heated by two halogen bulbs mounted in the main chamber and are thus kept at the same temperature. The temperature is measured with a Pt100

temperature sensor mounted at the collision chamber. Anions formed are extracted out of the collision chamber by a weak electric field and are mass analyzed with a quadrupole mass spectrometer (QMS). The mass analyzed ion current is amplified by a channel electron multiplier in single pulse counting mode and is recorded using a computer. With this setup the ion intensity for mass selected anions is recorded as a function of electron energy. The electron energy scale is calibrated with the s-wave resonance of SF_6^-/SF_6 [6]. The width of the corresponding resonance near 0 eV is also used for the determination of the electron energy resolution. SF_6 was introduced simultaneously with $CHCl_3$ into the chamber after a careful check that no interference between both compounds occurs. When changing the temperature, special emphasis was taken on constant performance of the monochromator (energy resolution and amount of zero electrons) which was monitored with SF_6^-/SF_6. In the case of deterioration the monochromator was retuned. The background pressure in the main chamber is 1×10^{-7} mbar measured with an ionization gauge. During measurements with chloroform the pressure in the chamber is 2×10^{-6} mbar.

2.4. Laser photoelectron attachment experiment (Kaiserslautern)

In order to measure highly resolved cross sections for anion formation in low-energy electron collisions with $CHCl_3$, we used two variants of the Laser Photoelectron Attachment (LPA) method, as discussed elsewhere in detail [6,55–57]. The energy range 1–200 meV was covered at a resolution of about 3 meV by the standard LPA method [6,55]: energy-variable photoelectrons (typical current 40 pA) are created in the reaction region with the target gas by resonant two-color photoionization of ground-state potassium atoms via the excited $K(4p_{3/2})$ level [56]. Higher electron energies were accessed by the Extended Laser Photoelectron Attachment (EXLPA) method [57]: here near-zero energy photoelectrons are produced in an auxiliary photoionization chamber (distance from reaction centre about 5 cm), accelerated by a weak electric field in a guiding magnetic field (0.002 T), brought to the energy of interest prior to traversal through the target region, and subsequently accelerated and deflected onto a collector plate. Care was taken to align the exciting and the focused ionizing laser (diameter 0.12 mm) to avoid any collisions of the electron beam with surfaces on its way from the photoionization chamber to the collector since these would yield spurious low-energy electrons and thus lead to unwanted attachment processes. This is especially critical in energy ranges where the attachment cross section is small. In this way, the drop of the SF_6^- cross section, for example, could be followed over five orders of magnitude towards higher electron energies [57]. The effective resolution in the EXLPA experiment was about 20 meV.

Both the LPA and the EXLPA experiment were pulsed at a rate of 100 kHz: following each photoelectron production and attachment period, the infrared laser (767 nm), exciting the $K(4s–4p_{3/2})$ transition, was switched off by an acousto-optical modulator, and a voltage pulse was initiated to extract the anions. A stack of electrodes imaged the anions onto the entrance hole of a quadrupole mass filter which mass selected the species of interest. The transmitted anions were detected by a channel electron multiplier (Fa. Sjuts, background 0.02/s).

A diffuse low density target of $CHCl_3$ molecules (Merck Co. 99% $CHCl_3$, stabilized by 1% Ethanol) at the gas temperature $T_G = 300$ K was used; gas chromatography revealed the presence of 0.1% CCl_4 in the sample. In view of the large DEA cross section for the process Cl^-/CCl_4 at low energies (thermal attachment rate coefficient $k(300\,\mathrm{K}) = 3.79(19) \times 10^{-7}\,\mathrm{cm^3\,s^{-1}}$ [15]) the raw attachment spectrum for $Cl^-/CHCl_3$ was corrected for this 0.1% contribution due to CCl_4, using the known attachment cross section for CCl_4 [58].

The LPA/EXLPA experiment provides a highly resolved yield $Y(E)$ for anion formation. This yield is proportional to the absolute DEA cross section, i.e., $\sigma(E) = N\ Y(E)$ where N is a normalization factor, assumed to be independent of electron energy E. The size of the normalization factor is established with reference to a known thermal DEA rate coefficient for the same process. The thermal rate coefficient $k = \langle v_{rel}\sigma(v_{rel})\rangle$ (v_{rel} = relative collision velocity of the electron-molecule system) is given by the average [2,5,6]:

$$k(T_e, T_G) = \left(\frac{2}{m}\right)^{1/2} \int E^{1/2}\, \sigma_{tot}(E; T_G)\, f(E; T_e)\, dE \tag{4}$$

Here, T_G denotes the rovibrational temperature of the target gas, T_e the electron temperature and $f(E;T_e)$ the electron distribution function. Note that the velocity of the gas molecules at $T_G = 300$ K is much smaller than the electron velocity even at electron energies as low as 0.1 meV, and the relative collision velocity v_{rel} can be replaced by the electron velocity. In calculating the rate coefficient, we use a Maxwellian distribution function which is given by:

$$f(E; T_e) = 2\left(\frac{E}{\pi}\right)^{1/2} \beta^{-3/2}\, \exp\left(\frac{-E}{\beta}\right) \tag{5}$$

with $\beta = k_B T_e$ (k_B = Boltzmann constant). The usual thermal average implies $T_e = T_G$ in (4). In the calibration of the absolute DEA cross section scale, we have used the thermal rate coefficient $k(T)$ measured for $T = T_e = T_G = 300$ K.

3. R-matrix calculations of the DEA cross section for Cl^- formation from $CHCl_3$

With the aim to provide some insight into the electron attachment process we have carried out semiempirical R-matrix calculations of the DEA cross sections. Low-energy inelastic electron scattering by chloroform is dominated by a shape resonance of a_1 symmetry [9,43]. One should expect that this resonance drives only totally symmetric vibrations: C—H stretch, symmetric C—Cl stretch, and symmetric CCl_3 deformation. However, dissociation of Cl^- is an asymmetric process, therefore for a rigorous calculation of the DEA process a multimode treatment, including the interaction between the vibrational modes, is necessary. In the present work, in order to describe the correct threshold behaviour of the DEA cross section, we employ the R-matrix method [59], and because of its complexity we use the one-mode approximation. First we identify the symmetric vibrational mode which is most important for the DEA process. Based on the observation of a direct anion dissociation process following Rydberg electron transfer to $CHCl_3$ [48] and the present experimental finding of a substantial channel interaction between the primary attachment process and vibrational excitation of the symmetric CCl_3 deformation mode ν_3 (see Section 4.2), we assume that the electron capture initially drives the ν_3 mode and that the primary temporary anion state is stabilized rapidly by motion along the ν_3 coordinate. Then, mediated by intramolecular vibrational energy redistribution (IVR), the excess energy is channeled into the C—Cl stretch which eventually leads to the dissociation into the fragments Cl^- and $CHCl_2$. The attachment process is thus treated in a one-dimensional approximation, assuming coupling of the anion state with only the ν_3 mode. This approach is similar to our effective-range-theory treatment of electron attachment to SF_6 [60].

The dominance of the ν_3 mode in the DEA process is confirmed by a vibrational mode analysis [61] employing the density functional approach with the hybrid B3LYP functional and the 6-31G(d) basis set. It shows that the amplitude of vibration of the Cl atoms is about three times greater in the ν_3 mode than in the symmetric

stretch ν_2 mode. The latter affects mostly the motion of the C—H complex.

We represent the neutral molecule by an effective one-dimensional potential energy curve generating the correct quantum of the ν_3 vibration, $\omega(\nu_3) = 45.0$ meV [62]. We use the reduced effective mass ($M = 21.29$ u [61]) for the ν_3 motion and the dissociation energy $D_{298}(CHCl_2–Cl) = 3.22(2)$ eV, as measured at $T = 298$ K [18]. Using the input data described above, we parameterize the neutral curve in the Morse form

$$V(\rho) = D_e[\exp(-a\rho) - 1]^2 \quad (6)$$

where $\rho = R - R_e$ is the normal ν_3 coordinate relative to the equilibrium separation R_e, $D_e = D_{298} + \omega(\nu_3)/2$, and $a = 0.6721 a_0^{-1}$ (a_0 = Bohr radius = 52.9 pm). The anion curve is parameterized in the form

$$U(\rho) = B\exp(-2b\rho) - C\exp(-b\rho) + F \quad (7)$$

The asymptotic value of the anion curve ($F = -0.370$ eV) was obtained from the dissociation energy D_e and the well-known electron affinity $EA(Cl) = 3.6127$ eV [17]. All other parameters were considered as empirical.

The R-matrix surface amplitude $\gamma(\rho)$ which determines the resonance width [59,63], was parameterized in the form

$$\gamma(\rho) = \frac{\gamma_0}{[\exp(\zeta\rho) + \eta]} \quad (8)$$

where γ_0, ζ and η are fit parameters. Typically, $\gamma(\rho)$ is a slowly varying function, and its value between the equilibrium separation ($\rho = 0$) and the crossing point between the neutral and the anion potential curves determines the absolute magnitude of the DEA cross section. The parameters employed in our calculations for the anion curve are $b = 0.4227 a_0^{-1}$, $B = 2.941$ eV, $C = 2.008$ eV, resulting in a (classical) barrier height (energy of the crossing point between $V(\rho)$ and $U(\rho)$ above the minimum of the neutral potential) of 0.121 eV. The parameters of the surface amplitude were obtained as $\gamma_0 = 0.4735$ ($a_0 \times$ Hartree)$^{1/2}$ (1 Hartree = 27.211 eV), $\zeta = 7.828 a_0^{-1}$, and $\eta = 3.043$. The vibrational motion for the calculation of the DEA cross sections was included, using the quasiclassical approximation of the R-matrix theory [59,64]. To couple the resonant anion state with the electron continuum, we calculate the electron wave functions in electron scattering channels. For these calculations we have employed the dipole moment of $CHCl_3$ $\mu = 1.04$ D [18] and the polarizability $\alpha = 64 a_0^3$ [18].

4. Results and discussion

4.1. Thermal attachment rate coefficients for $CHCl_3$

In the swarm experiments carried out at Siedlce, thermal rate coefficients $k(T)$ for the electron capture process by $CHCl_3$ molecules have been measured over the temperature range $T = 295$–373 K. Note that T refers to both the gas temperature T_G and the electron temperature T_e which have the same value at all T in the present swarm experiments.

At room temperature ($T = 295$ K) the rate coefficient was determined from several measurements as $k(295\text{ K}) = 3.7 \times 10^{-9}$ cm^3 s^{-1} with an estimated overall uncertainty of ±5%. The previously reported (near) thermal rate coefficients ($T = 293$–300 K) range from 1.3×10^{-9} to 4.9×10^{-9} cm^3 s^{-1} (see Table 1). The results obtained with electron swarms either in drift tubes or in flowing afterglows (combined with ECR or Langmuir probe detection) fall into the narrower range $(3.6$–$4.9) \times 10^{-9}$ cm^3 s^{-1} [25,26,33,34,36–38]. From an analysis of electron beam attachment data [9], taken with $CHCl_3$ gas at a temperature of 338 K, Gallup et al. [11] derived an estimate for the rate coefficient of 9.4×10^{-9} cm^3 s^{-1}; our value at $T = 338$ K is 6.3×10^{-9} cm^3 s^{-1} which can be considered as satisfactory agreement in view of the uncertainties of the effective electron energy distribution function at near zero electron energy (see also discussion below).

Table 1
Thermal electron attachment rate coefficients $k(T)$ and activation energies E_a for $CHCl_3$

T (K)	$k(T)$ (10^{-9} cm^3 s^{-1})	E_a (eV)	Reference; method
295	3.7 ± 5%	0.11(1)	Present
300	3.9		Pulsed Townsend
340	6.9		Carrier Gas CO_2
298	4.9		[25] (see also [26,32]); Swarm, CG N_2
≈296	3.8		[26] (see also [16,32]); Swarm, CG N_2
298 or 299	2.3(2) (four values quoted, ranging from 2.0 to 3.8)		[32]
		0.134(9)	[27] Pulse sampling
300	2.2–2.6	0.095	[28] ([32]); Microwave, CG n-C_6H_{14}
293	1.3	0.10	[31]; ECR, CG Ar
300	2.2/2.6	0.10_4	[30]; ECR, CG Ar
300	4.4 ± 15%	0.11(1)[a]	[33]; FALP, CG He
293	3.8		[34]; FA-ECR, CG He(Ar)
300	2.0 ± 15%		[35]
		0.13(1)	[23] MWPR-MH, CG Xe
300	3.6 ± 15%		[36,38]; FALP, CG He or Ar
293	4.7	~0.06	[37]; FA-ECR, CG He + Ar

[a] From fit to data listed in [33]; these authors quoted 0.12 eV.

Over the temperature range $T = 295$–373 K, a strong increase in $k(T)$ is observed (see Fig. 1a) which exhibits Arrhenius-type behaviour, as shown in Fig. 1b. From the fit to the data points with a function $k(T) = A\exp[-E_a/(k_B T)]$ (A = constant) the activation energy was determined as $E_a = 0.11(1)$ eV. This value is in good to fair agreement with previous determinations [23,27,28,30–33] (see Table 1)

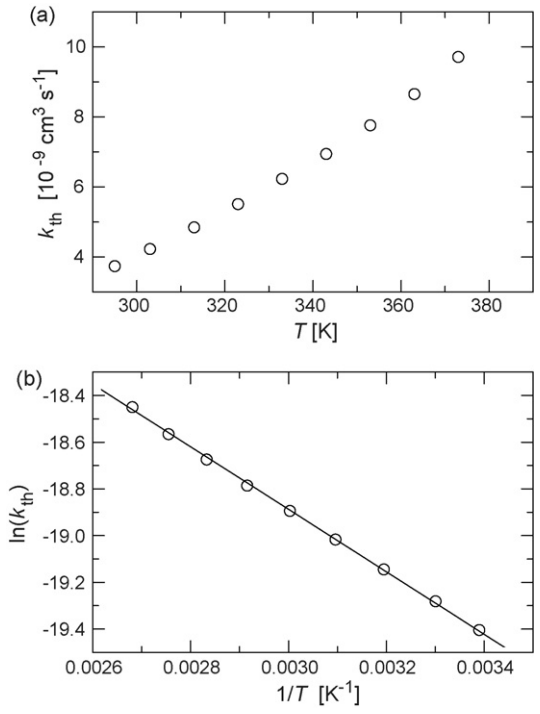

Fig. 1. (a) Dependence of the thermal electron attachment rate coefficient $k(T)$ on temperature for $CHCl_3$. (b) Arrhenius plot of the rate coefficient $k(T)$ for electron attachment to $CHCl_3$. The full line is the fit to the data points, yielding the activation energy $E_a = 0.11(1)$ eV.

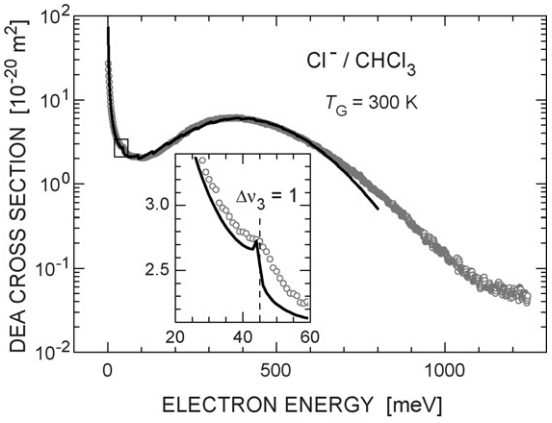

Fig. 2. Absolute cross section for Cl^- formation due to electron attachment to $CHCl_3$ (gas temperature T_G = 300 K). Open circles: combined LPA/EXLPA cross section over the range 0.001–1.25 eV. Full curve: result of R-matrix calculation (not convoluted with the experimental resolution). The insert presents a magnified view of the downward step-like structure which occurs at the threshold for vibrational excitation (VE) of one quantum of the $\nu_3(a_1)$ mode (≈45 meV) and which is due to interaction between the attachment and the VE channel.

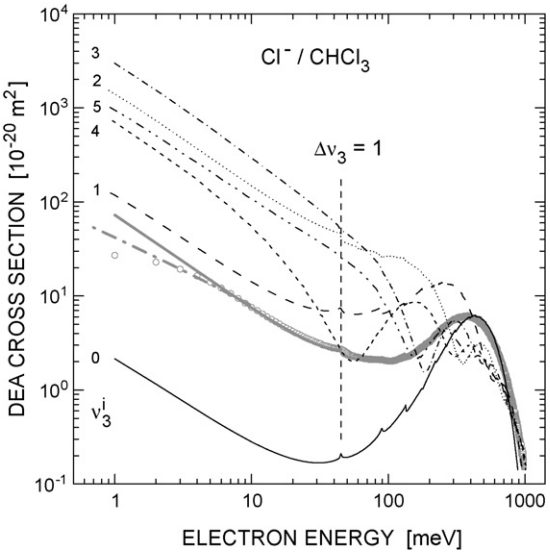

Fig. 3. Calculated state-specific partial absolute DEA cross sections for $CHCl_3$ molecules in the initial vibrational level $\nu_3^i = 0-5$ (indicated curves drawn with different line styles). The measured DEA cross section is shown by the grey open circles and the calculated thermal vibrational average (T_G = 300 K) by the bold grey line. The grey chain line represents the EVW cross section, normalized to the experiment at E = 3 meV.

while the estimate $E_a \approx 0.06$ eV from the data in [37] appears to be too low.

4.2. Highly resolved absolute cross section for Cl^- formation in DEA to $CHCl_3$ molecules (T_G = 300 K) and comparison with R-matrix theory

In agreement with the earlier work [39,41,42,44–46], the present experiments in Belfast, Innsbruck, and Kaiserslautern confirm that Cl^- is by far the dominant anion formed in low-energy electron attachment to $CHCl_3$. In the following we discuss the highly resolved LPA and EXLPA results which were obtained for the Cl^- anion over the range 0.001–1.25 eV. With reference to the present thermal rate coefficient $k(300\,K) = 3.9(2) \times 10^{-9}\,cm^3\,s^{-1}$, the absolute scale for this partial DEA cross section was determined which is subsequently used to establish absolute cross sections also for the two fragment anion channels HCl_2^- and CCl_2^- and for total anion production.

In Fig. 2, we present the absolute DEA cross section for Cl^- formation due to electron attachment to $CHCl_3$ (gas temperature T_G = 300 K) determined in this work by combining the LPA (0.001–0.19 eV) and the EXLPA (0.19–1.25 eV) data. The energy resolution was about 3 meV for the LPA data and about 20 meV for the EXLPA results. The LPA anion yield was averaged over nine original data points (about 10 channels/meV) and interpolated with respect to an integer meV scale; the EXLPA anion yield was measured with a channel width of 1 meV and normalized to the LPA data in the energy range from 70 to 180 meV where the LPA and EXLPA yields exhibited the same shapes (with a minimum at 104 meV). Below about 1 eV the partial Cl^- cross section is identical with the total cross section since other fragment ions do not contribute at a significant level (see below); therefore, it is possible to use the *total* thermal rate coefficient $k(T = 300\,K)$ to establish the absolute cross section scale shown in Fig. 2.

Close to E = 45 meV, a clear downward-step like Wigner cusp is observed (see inset in Fig. 2) which is attributed to the interaction of the primary attachment process with the channel for VE of one quantum of the $\nu_3(a_1)$ mode (fundamental frequency 363 cm^{-1} = 45.0 meV [62]). (The sharp cusp in the calculated cross section occurs at an energy slightly below 45.0 meV because the dominant contributions to the DEA cross section stem from the initial $\nu_3^i = 1$ and 2 levels for which the onsets for the $\Delta\nu_3 = 1$ vibrational transitions occur below 45 meV as a result of anharmonicity effects.) As is known from the previous high resolution work on molecules such as SF_6 [6,57], CCl_4 [58], CF_3Br [20], and CF_3I [65], these Wigner cusps are characteristic for the vibrational modes which are active in the attachment process. Note that for Cl^- formation, the vibrational modes which may be considered to promote dissociation of the primary anion complex $[CHCl_3]^-$ towards the fragments $Cl^- + CHCl_2$ are not identical with the channel interaction mode $\nu_3(a_1)$ which represents the CCl_3 symmetric deformation mode with a_1 symmetry which is compatible with s-wave electron attachment.

The observation of the cusp structure at the $\Delta\nu_3(a_1) = 1$ vibrational onset was incorporated into our theoretical model, whose results are included in Fig. 2 and presented in more detail in Fig. 3. We note that the cross section calculated for T_G = 300 K represents the appropriate vibrational average with regard to the initial thermal population of the $\nu_3(a_1)$ mode. At T_G = 300 K, the relative initial populations in the $\nu_3^i = 0$–3 levels are given by 100, 17.5, 3.1, and 0.54, respectively. Since the DEA cross sections for $\nu_3^i = 1, 2,$ and 3 are much larger than that for $\nu_3^i = 0$ at energies below 0.2 eV as a result of more favourable Franck–Condon factors for the transition from the neutral to the anion state, the $\nu_3^i = 1, 2,$ and 3 levels contribute to the DEA cross section at a significant level in spite of their minor populations.

In the calculated state-specific cross sections, sharp Wigner cusp-type structure of different shape is observed at the onsets for vibrational excitation of one or more quanta of the symmetric deformation mode ($\Delta\nu_3^i \geq 1$). Moreover, wider oscillatory structure is observed which is attributed to the effects of the nodal structure in the vibrational wave functions for $\nu_3^i \geq 1$.

At low electron energies, we compare the measured cross section *shape* with the prediction of the extended Vogt-Wannier (EVW) capture model [5,66] (grey chain curve in Fig. 3), using the electric dipole moment and the polarizability given above. The predicted EVW cross section is a factor of 100 larger than the measured absolute DEA cross section, indicating – in contrast to, e.g., the cases of SF_6 or CCl_4 [5,66] – that for the molecule $CHCl_3$ the efficiency for anion formation only amounts to 1% of the electron capture

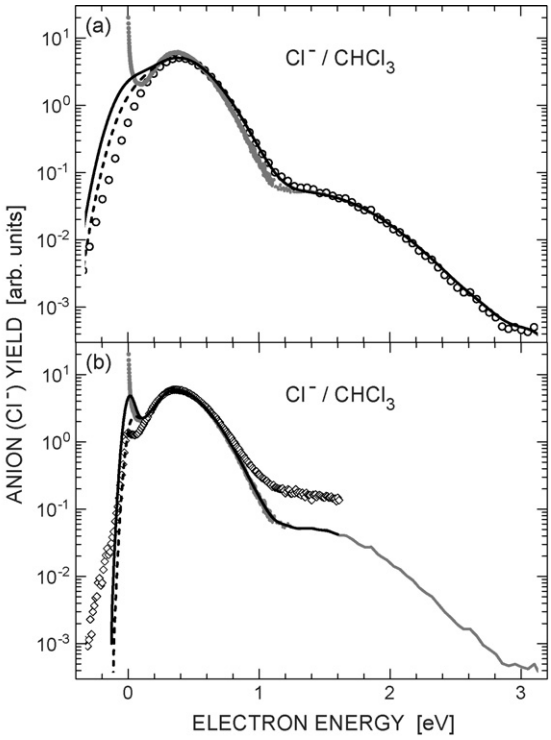

Fig. 4. Comparison of the highly resolved LPA/EXLPA yield (grey data points) for Cl^- formation from $CHCl_3$ with (a) the TEM-TOF results (Belfast, open circles) and (b) the HEM-QMS results (Innsbruck, open diamonds). For details see text (gas temperature close to T_G = 300 K).

events. In the R-matrix description of the DEA process, the EVW cross section behaviour is built into the theory via the long-range electron-molecule interactions. The lowering of the DEA cross section from the EVW value is due to two effects: (i) non-optimal Franck–Condon factors for the transition from the neutral molecule to the initial temporary negative ion (TNI) state upon electron capture; (ii) a smaller than unity survival probability for the evolution of the TNI to the dissociated pair $Cl^- + CHCl_2$.

According to the threshold law for exothermic reactions at very low energies [66], the DEA cross section should be proportional to E^{-X} where the threshold exponent X depends on the molecular dipole moment. For the $CHCl_3$ molecule one obtains $X = 0.623$. As observed in Fig. 3, the state-specific and the vibrationally averaged R-matrix cross sections are distinctly steeper at very low energies. This can be explained by the presence of a weakly bound or a virtual state due to the combined dipolar and polarization interactions, making the region of validity of the threshold law extremely narrow. For the methyl iodide molecule, for example, the calculated DEA cross section grows much faster towards lower energies than predicted by the EVW threshold law and reaches the correct slope only in the region below 0.1 meV [66]. A similar effect is observed in the present case. However, whereas in the methyl iodide case this effect is caused by a bound state leading to the vibrational Feshbach resonance (VFR) below the first vibrational excitation threshold [67], in the case of chloroform no evidence for a VFR and a bound state is present, therefore the effect is due to a virtual state. We should note also that the discussed behaviour is pertinent to collisions with molecules with fixed orientation. In reality the molecules rotate, and when rotation is taken into account, the Bethe-Wigner law $\sigma(E \to 0) \propto E^{-1/2}$ should be restored in the sub-meV region [66].

In Fig. 4 we compare the yield for Cl^- formation from three different experiments over the energy range from −0.4 to 3.1 eV. In the two diagrams (a) and (b), the small full circles (grey) represent the combined LPA/EXLPA anion yield (0.001–1.1 eV, taken from Fig. 2). It is extended to higher energies by a brief interpolation over the range 1.1–1.5 eV (which can be regarded as a deconvoluted cross section around the fairly sharp bend near 1.1 eV); it merges into the broadly shaped Belfast data at energies above 1.5 eV (open circles in Fig. 4a). For better visibility, the resulting joint Cl^- yield (E = 0.001–3.1 eV) is displayed in Fig. 4b by the grey full dots (LPA/EXLPA) and the grey full curve (Belfast data above 1.5 eV), respectively. This joint Cl^- yield, when normalized to the thermal rate coefficient as discussed in connection with Fig. 2, represents our new absolute cross section for Cl^- formation from $CHCl_3$ at T_G = 300 K.

In Fig. 4a we compare the yield measured with the Belfast TEM-TOF apparatus (open circles) with the yield (full curve), obtained by convolution of the joint Cl^- yield with a Gaussian of FWHM = 0.27 eV (full width at half maximum), chosen to provide an adequate description of the Belfast results at electron energies above 0.2 eV. At energies below about 0.2 eV, the Belfast data deviate substantially from this convoluted yield. This deviation is not the result of an improper choice of the FWHM of the resolution function, but rather due to the fact that the Belfast measurement missed the energy range close to 0 eV. If the joint yield is truncated (i.e., set to zero at energies below 0.01 eV) to approximately account for this effect, the convolution with the same Gaussian (FWHM = 0.27 eV) leads to the broken curve which is somewhat closer to the measured data points at low energies. We note that the original energy scale of the Belfast data was shifted by 0.1 eV to optimally match that of the convoluted spectrum.

In Fig. 4b, we compare the data measured at Innsbruck with the HEM-QMS setup at T_G = 310 K (open diamonds) with the yield (full black curve), obtained by convolution of the joint Cl^- yield with a Gaussian of FWHM = 80 meV. The energy scale of the Innsbruck data is shown as obtained with reference to the zero energy peak for SF_6^- formation from SF_6, see Section 2.3. The respective anion yields are normalized to the same value at the maximum around 0.37 eV. In addition, we show the yield (broken curve) which results by convolution of the truncated joint Cl^- yield (cross section set to zero at energies below 0.01 eV). Good agreement between the shapes of the LPA/EXLPA yield and the HEM-QMS yield is observed over the range 0.2–0.8 eV (considering the uncertainty of the absolute energy scale of the latter of about 0.03 eV). Substantial deviations are, however, observed near 0 eV and towards larger energies where the Innsbruck yield progressively stays above the joint LPA/EXLPA/Belfast anion yield (by about a factor of 3 at energies above 1.3 eV). The latter difference is attributed to 'background' which is probably due to anion formation involving slow electrons resulting from inelastic scattering at metal electrodes.

At near-zero energy, the yield measured with the HEM setup stays substantially below the convoluted LPA anion yield. We attribute this difference to the difficulty in reaching zero energy with a decelerated electron beam, especially in the absence of a guiding magnetic field. Even in the presence of a guiding magnetic field, transverse velocity components prevent the range close to zero kinetic energy being accessed; moreover, electron spiralling effects introduce uncertainties in the pathlength and thus in the anion yield. Even if transverse components are ruled out or reduced (as in the EXLPA experiment in which the photoelectrons are formed with zero kinetic energy), there is still the uncertainty whether the electrons are decelerated to near-zero energy in the proper reaction volume and whether the electrons traverse this volume only once. In our opinion, the only trustworthy, presently available approach to reliably measure the shape of DEA cross sections at energies below about 50 meV is the laser photoelectron attachment experiment in which monoenergetic electrons with

variable kinetic energy undergo attachment reactions in essentially the same (nearly) field-free volume in which they are formed by photoionization.

4.3. Absolute cross section for CCl_2^- and HCl_2^- formation in DEA to $CHCl_3$ molecules

In Fig. 5 we present the absolute partial cross sections for DEA to $CHCl_3$, resulting in CCl_2^- (Fig. 5a) and HCl_2^- production (Fig. 5b). These data were measured with the Belfast TEM-TOF apparatus simultaneously with the partial yield for Cl^- formation. Test measurements suggest that the relative detection efficiencies of these three anions at the multichannel plates were the same to within 20%. In principle, the detection efficiencies at multichannel plates should increase with the kinetic energy of the incident ion until a plateau is reached. Ions of different masses with the same kinetic energy will, however, strike the detector with different velocities which may lead to lower detection efficiencies for heavier ions. Variation of kinetic energy of the ions striking the multichannel plate detector in the TOF apparatus by a factor of 8 did not significantly alter the relative intensities of ions of different masses observed under otherwise identical conditions. There should be little discrimination against ions ejected in fragmentation with different kinetic energy releases because a field of 200 V/cm was used to extract ions from the interaction region of the TOF apparatus.

The absolute cross section scale for Fig. 5 is deduced from the respective relative anion intensities and the absolute cross section scale for Cl^- formation (Figs. 2 and 4). The shape of both bands is well described by Gaussians with nearly identical widths, located at 1.72(2) eV for CCl_2^- (FWHM 0.79(1) eV) and at 1.84(3) eV for HCl_2^- (FWHM 0.78(2) eV). As already mentioned in the introduction, the anions CCl_2^- and HCl_2^- are both formed through the first excited negative ion resonance with ^2E symmetry.

In Table 2, we summarize the information on the energy location, the relative intensity, and the energy-integrated cross section of the bands for the three anions Cl^-, CCl_2^- and HCl_2^-, as obtained in the present work at Belfast and Innsbruck, and compare it with that of previous studies [41,42,46]. With regard to the energy locations, good agreement is found between the two present sets of results, (i.e., set (I): Belfast, Kaiserslautern, and set (II): Innsbruck), with which those of the Oak Ridge group (read from Fig. 3a in Ref. [41]) are compatible. Compared to the present values, the peak energies of the Berlin group [42] for CCl_2^- and HCl_2^- are too low

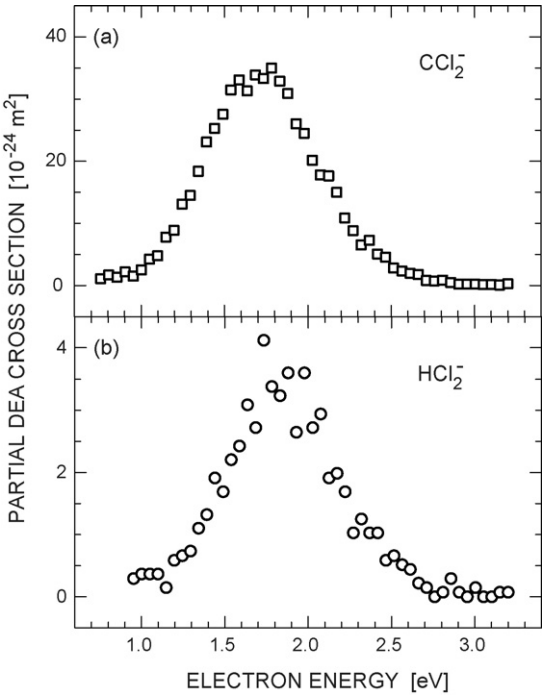

Fig. 5. Absolute partial cross section for (a) CCl_2^- formation and (b) HCl_2^- production due to electron attachment to $CHCl_3$ molecules at the gas temperature T_G = 300 K.

Table 2
Peak positions, branching ratios and energy-integrated partial cross sections for the formation of Cl^-, CCl_2^-, and HCl_2^- in DEA to $CHCl_3$

Anion	Peak position (eV)	Peak width (FWHM) (eV)	Peak Maximum (10^{-20} m^2)	Branching ratio (max.)	Integration range (eV)	Integral (10^{-20} m^2 eV)	Branching ratio (integral)
Cl^-							
(I)[a]	0.375(5)[b]	0.41(1)[b]	6.1(5)[b,c]	1000	0–3.2	3.2(2)[c]	1000
(II)	0.37(1)[b]	0.44(2)[b]					
[41][d]	≈0.35						
[46]	0.3						
[42]	0.32(5)[f]						
CCl_2^-							
(I)	1.72(2)[e]	0.79(1)[e]	3.4×10^{-3}[e]	0.56	0.76–3.2	2.9×10^{-3}	0.91
(II)	1.70(5)			1.5			2.5
[41][d]	≈1.65			0.97			
[46]	1.56			8.6			
[42]	1.45(10)						0.7
HCl_2^-							
(I)	1.84(3)[e]	0.78(2)[e]	3.4×10^{-4}[e]	0.056	0.95–3.2	2.9×10^{-4}	0.091
(II)	1.81(6)			0.13			0.2
[41][d]	≈1.8			0.12			
[46]	1.71			0.9			
[42]	1.61(1)						2.0

The branching ratios are based on isotope-summed intensities. (I): combined LPA/EXLPA and Belfast data (T_G = 300 K), (II) Innbsruck data (T_G = 310 K).

[a] From the combined partial cross section (see Fig. 4).

[b] Peak position, maximum, and width are given for the second broad peak.

[c] Error bar due to uncertainties of (i) thermal rate coefficient used for calibration of absolute cross section scale [5%], (ii) 0.10(5)% contamination by CCl_4 [6%], and (iii) extrapolation for E < 1 meV [2%].

[d] Evaluated from Fig. 3a of [41] (the anions CCl_2^- and HCl_2^- were incorrectly addressed as $HCCl_2^-$ and Cl_2^-, respectively).

[e] From a Gaussian peak fit to the data of Fig. 5.

[f] According to Fig. 5 of [42] located at ≈0.21 eV.

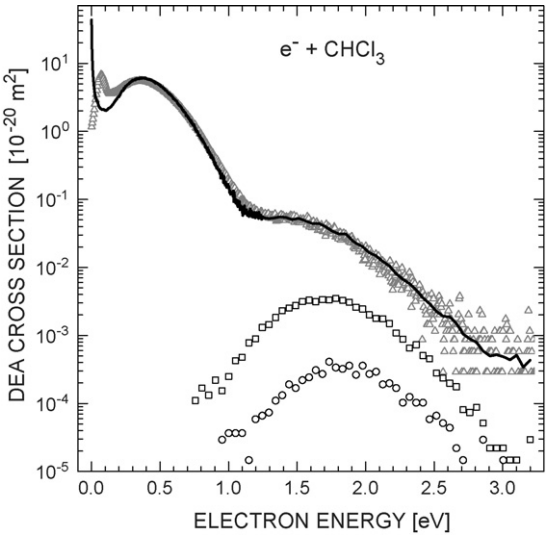

Fig. 6. Total (full line) and partial absolute cross sections for anion formation in electron-$CHCl_3$ collisions (gas temperature T_G = 300 K); CCl_2^-: open squares; HCl_2^-: open circles. The open triangles represent the total DEA cross section, deduced from the results of Aflatooni and Burrow [9] ($T_G \approx 338$ K) in modified form (see text).

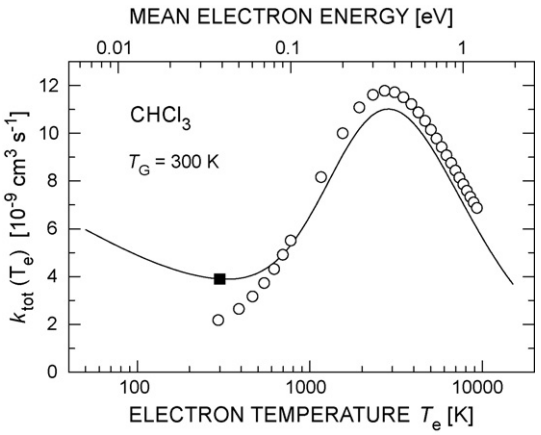

Fig. 7. Dependence of the total rate coefficient for DEA to $CHCl_3$ on electron temperature T_e over the range 50–15,000 K (mean electron energy $\langle E \rangle$ = 0.0065–1.94 eV) at the fixed gas temperature T_G = 300 K. Full curve: rate coefficients calculated from the total DEA cross section in Fig. 6 open circles: electron swarm results (MWPR-MH method) from [23]. The full square denotes the thermal rate coefficient (3.9×10^{-9} cm^3 s^{-1} at $T_e = T_G$ = 300 K) which was used for calibration of the DEA cross section (see text).

by 0.2–0.25 eV while the earlier results of the Innsbruck group [46] are lower by 0.1–0.15 eV.

With regard to the branching ratios for the band maxima and for the energy-integrated band intensities (normalized to 1000 for Cl^-), the Belfast results agree with the present Innsbruck data and with the Oak Ridge data [41] to within a factor of 2–3 while the branching ratios reported by Dorman (ratio of peak maxima 1000:300:100, see caption of Fig. 2 in [39]), and those given in [42], and [46] show larger deviations. These differences are mainly attributed to systematic errors which are likely associated with incomplete anion collection. Another possible source of error for the data quoted in [46] may be pressure instabilities. As absolute partial energy-integrated cross sections for the three anions Cl^-, CCl_2^- and HCl_2^- (energy range up to 3.2 eV) we recommend the values (3.2, 2.9×10^{-3}, 2.9×10^{-4}) $\times 10^{-20}$ m^2 eV, respectively.

4.4. Total cross section for DEA to $CHCl_3$ (T_G = 300 K) and the dependence of the DEA rate coefficient on electron temperature

Summation of the three partial absolute DEA cross sections in Figs. 2, 4, and 5 yield the total absolute DEA cross section $\sigma_{tot}(E)$ for $CHCl_3$, shown as the full curve in Fig. 6 over the energy range 0.001–3.2 eV. For comparison, we included the partial cross sections for CCl_2^- (open squares) and HCl_2^- formation (open circles). We neglect the other very weak anion channels, detected by Denifl et al. [46] (see above). The Cl^- channel (not shown in Fig. 6) is found to dominate throughout the energy range covered in Fig. 6, i.e., also in the range of the first excited ^2E resonance. Over the broad energy range 0.2–3.2 eV, our total cross section is in very good agreement with the cross section shown by the open triangles, as obtained from the absolute total DEA cross section of Aflatooni and Burrow [9] ($T_G \approx 338$ K) by imposing two modifications: (i) a shift of the latter to higher energies by 0.07 eV, and (ii) a multiplication of the absolute scale of the data reported in [9] by a factor of 0.58. The energy shift is justified by the observation (see Section 4.5) that the location of the peak observed at 0.37 eV in the LPA/EXLPA measurement shifts by only 11 meV to lower energy when the gas temperature is raised to 340 K (see Figs. 8 and 9), and thus (most of) the deviation between the peak locations in the LPA/EXLPA data and the TEM data of Aflatooni and Burrow cannot be caused by the difference in gas temperature. Instead we suggest that this deviation is mainly due to the fact that this TEM measurement did not access energies close to 0 eV (see also the discussion above). The ≈40% deviation in the absolute size of the two total DEA cross sections is only in part covered by the uncertainties of the TEM result (10%) [9] and of the rate coefficient (5%) to which the LPA/EXPLA data have been normalized. An independent future measurement of the absolute DEA cross section or of the thermal rate coefficient would be desirable to shed light on the source of this difference.

In the following, we discuss the dependence of the total DEA rate coefficient $k(T_e;T_G)$ on electron temperature T_e for the fixed gas temperature T_G = 300 K. We calculate $k(T_e;T_G)$ with (4), using the total DEA cross section in Fig. 6 and a Maxwellian electron distribution function. The latter choice appears to be justified for the electron swarm experiment with varied electron temperature [23,35] with which we compare the calculated rate coefficients. Sunagawa and Shimamori [23,35] used the MWPR-MH (microwave cavity pulse radiolysis with microwave heating) method in which the electron temperature T_e in the carrier gas xenon can be changed by microwave heating at fixed gas temperature T_G.

In Fig. 7 we compare our calculated rate coefficients $k(T_e;T_G = 300)$ with the MWPR-MH results [23,35], as measured at T_G = 300 K. The two data sets show good qualitative agreement in the major feature, the maximum located at about $T_e \approx 2800$ K (mean electron energy $\langle E \rangle = (3/2)k_B T_e \approx 0.36$ eV). The MWPR-MH rate coefficient in this maximum exceeds the calculated value by only 7%. The MWPR-MH result for $T_e = T_G$ = 300 K [23,35], however, is almost a factor of 2 below the present thermal rate coefficient; the cause for this difference is not clear.

We note that Sunagawa and Shimamori [23] proposed a DEA cross section from an analysis of the T_e dependence of their rate coefficients measured at T_G = 300 K. This cross section is remarkably close to our total DEA cross section in shape and absolute value at electron energies above about 0.2 eV, but much too low at the lower energies.

4.5. The dependence of the relative cross section for Cl^- formation in DEA to $CHCl_3$ on the gas temperature (T_G = 310–435 K)

Using the Innsbruck HEM-QMS setup with a temperature-variable molecular beam source, we studied the dependence of

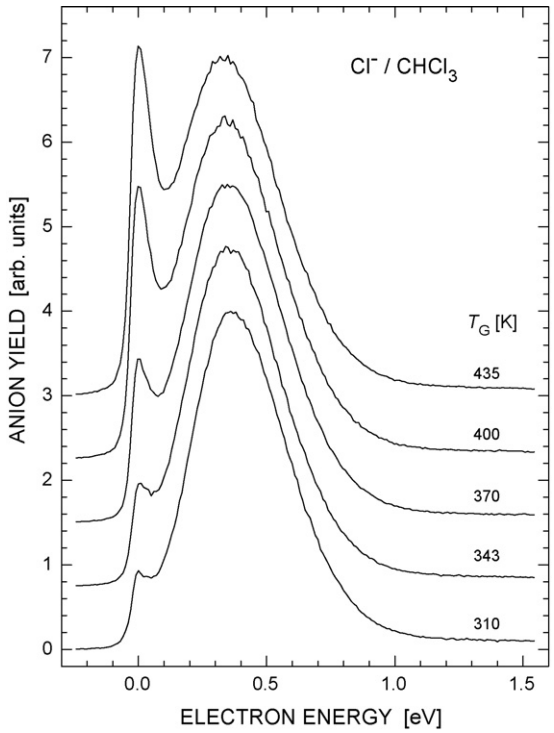

Fig. 8. Dependence of the Cl^- yield due to DEA to $CHCl_3$ (measured with the HEM-QMS setup, resolution about 80 meV) on the gas temperature over the range T_G = 310–435 K; the respective anion yields were normalized to the same value at the higher energy peak and are shifted by adding a constant offset to each subsequent spectrum for clarity.

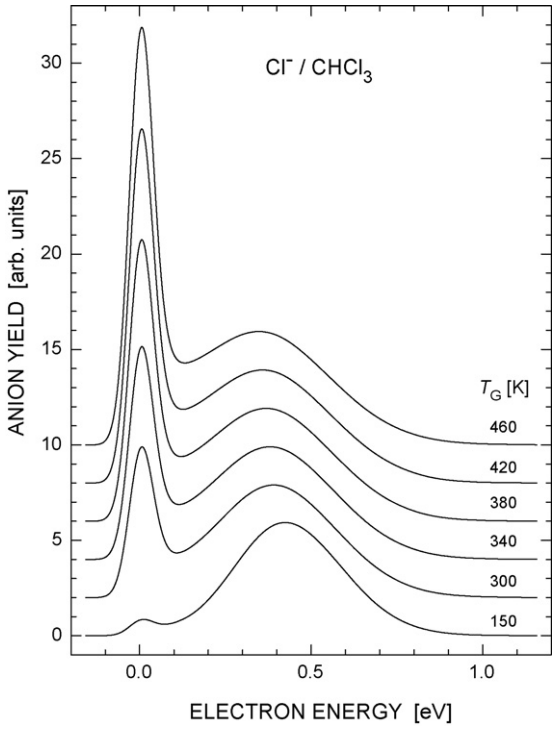

Fig. 9. Dependence of the calculated DEA cross section for Cl^- formation on the vibrational temperature T_G of the $CHCl_3$ molecules, as obtained by convolution with a Gaussian resolution function of 80 meV FWHM (T_G = 150–460 K); for clarity, the spectra are shifted vertically by a constant amount, respectively.

the yield for Cl^- formation from $CHCl_3$ on the gas temperature T_G over the range 310–435 K, i.e., on the rovibrational temperature of the molecules. The results are shown in Fig. 8; the anion yields (respectively shifted by a constant amount in the vertical direction for clarity) were normalized to the same value at the maximum (see comments and justification below), observed here at ≈0.37 eV for T_G = 310 K, in agreement with the LPA/EXLPA result. We note that in the previous TEM experiments the maximum of this peak occurred at 0.25 eV [44], 0.27 eV [45], and 0.30 eV [46]. It appears that the peak locations of these TEM data are all too low, probably as a result of the fact that these measurements did not really reach zero electron energy. We further mention that the maximum of the near-zero energy peak was placed at 0 eV in the previous data [44-46] as well as in the DEA spectra shown in Fig. 8. This choice is not appropriate for experiments with finite energy resolution [58,68]; in spectra obtained by convolution of the calculated cross sections with a Gaussian of 80 meV FWHM (see Fig. 9) the maximum of the near-zero energy peak is located at ≈7 meV which for the data in Fig. 8 is within the uncertainty of the overall energy calibration.

The shape of the broad band changes rather little with gas temperature at electron energies above 0.2 eV. The maximum position of the band exhibits a monotonical weak shift to lower energies with rising temperature (maximum location ≈0.33 eV at 435 K). In contrast, a clear rise is seen for the peak observed near zero energy in qualitative agreement with the previous observations [44,45]. An Arrhenius-type plot of the maximum intensity of the peak at near-zero energy yields an estimate for the (electron energy resolved) activation energy of 0.15(2) eV, somewhat higher than the thermal activation energies (0.11–0.13 eV), measured in swarm experiments for equal electron and gas temperature (see Table 1). The previous attempts to determine 'activation' energies' from the temperature variation of the near-zero energy peak (using magnetically guided electron beams) yielded estimates of 0.11(2) eV [44] and 0.08(2) eV [45]. Clearly, all these electron beam results are rather uncertain in view of the fact that maximum intensities for near-zero energy peaks, measured with decelerated electron beams (with or without a magnetic guiding field) are problematic, as discussed above. The 'activation energy' 0.08(2) eV reported in [45] is definitely too low; as discussed in [45], this low value arose most likely from thermal decomposition effects of chloroform at elevated gas temperatures (up to 550 K). The near-zero energy Cl^- ion yield reported in [44] should be viewed with caution; it exhibited already at room temperature a strongly enhanced yield near 0 eV (about 13 times higher than that for the second peak observed at 0.3 eV). Revisited measurements with ozone showed, however, that such enhanced yields near zero energy like those observed in [44] have to be attributed to an artifact due to multiple reflection of very low-energy electrons in the collision chamber of the trochoidal electron monochromator (see also the detailed discussion in [69]).

We add a remark on the comparison of thermal activation energies ($T_e = T_G$) with non-thermal results: recent work, e.g., on DEA to CH_3Br [24] has demonstrated that the thermal activation energy is significantly *smaller* than non-thermal values which result in experiments with electrons of average energies much *lower* than the gas temperature (as for instance measured by Rydberg electron transfer [24]).

A comparison of the total cross section for anion production reported by Aflatooni and Burrow at $T_G \approx 338$ K [9] with the HEM-QMS yield for Cl^- formation at T_G = 343 K (normalized to the same height at the peak around 0.37 eV) exhibits the following deviations: the near-zero energy peak in the HEM data is about a factor of 4 smaller while at energies above about 0.3 eV, they progressively stay above the total anion yield. The former observation reflects the tendency already reflected in the comparison between the HEM

data and the LPA results, namely that the HEM anion yield near zero energy is too low. The latter observation is partly due to the background in the HEM data (especially at energies above 1.2 eV), but also due to the fact that the maximum of the (original) TEM data [9] occurs at about 0.3 eV while the HEM data peak at about 0.36 eV for T_G = 343 K.

We add a comment on the temperature (in)dependence of the broad peak. In a recent study, covering the temperature range 300–550 K, Matejcik et al. [45] found that the intensity of this peak followed a $T_G^{-0.5}$ dependence for temperatures up to 420 K. Since the molecular density in the reaction volume is expected to vary as $T_G^{-0.5}$, this observation is compatible with a peak cross section which is *independent* of gas temperature, and we have used this independence in plotting the Innsbruck data in Fig. 8. Above about 470 K, Matejcik et al. found the overall signal to decrease which was ascribed to thermal decomposition of chloroform on the hot surfaces in the molecular beam source [45]. With the Innsbruck setup it was not possible to exceed the temperature 435 K, and hence thermal decomposition of chloroform did not play a role.

The fact that the maximum cross section for the broad peak is independent of gas temperature (as assumed in Fig. 8), is confirmed by the results of the R-matrix calculations which are shown in Fig. 9 for six vibrational temperatures, ranging from 150 to 460 K. The spectra have been convoluted with a Gaussian of 80 meV FWHM (simulating the resolution of the experimental results in Fig. 8).

The value of the calculated maximum cross section ($\approx 5.9 \times 10^{-20}$ m^2) of the broad peak is constant (to within 1%) over the range 150–460 K. As expected from the shapes of the DEA cross sections for the individual initial vibrational levels (see Fig. 3), the maximum position of this band shifts somewhat to lower energies with rising temperature (by −11 meV per 40 K temperature rise over the range 300–460 K), in good agreement with the experimentally observed shifts. For T_G = 150 K the maximum of the cross section occurs at 424 meV, i.e., it is shifted by 34 meV relative to the maximum for 300 K.

The near-zero energy peak of the convoluted theoretical spectra is much stronger (relative to the maximum near 0.37 eV) than that in the respective experimental Cl^- yield (Fig. 8); this reflects the fact that the near-zero anion yield is suppressed in the Innsbruck data. A semilog plot of the intensity of the near-zero peaks in Fig. 9 versus inverse gas temperature indicates Arrhenius-type behaviour with an 'energy-selected activation energy' of 76 meV, lower than both the present thermal activation energy and the 'energy-selected' value suggested by the Innsbruck data. A calculation of the thermal rate coefficient (4) with the calculated vibrationally averaged DEA cross sections yields a thermal activation energy of 62 meV; as expected, this value is somewhat lower than the energy resolved near 0 eV value of 76 meV. For comparison we note that the energy of the crossing point between the neutral and the (diabatic) anion curve lies 121 meV above the minimum of the neutral potential curve (i.e., 98.4 meV above the lowest vibrational level $\nu_3 = 0$). A recent theoretical investigation on the validity range of the Arrhenius equation for exothermic DEA to molecules [21] with an intermediate barrier (as in the present case) has demonstrated that the thermal activation energy typically is substantially smaller than the barrier height.

We conclude that the theoretical model underlying the R-matrix calculations provides a good description of the major experimental observations, i.e., the absolute DEA cross section, the energy location of the broad peak near 0.37 eV and the general variation of the DEA cross section with vibrational temperature. On the quantitative level, the calculations yield a weaker rise of the near-zero energy cross section with increasing vibrational temperature T_G and of the thermal rate coefficient $k(T)$ with increasing temperature $T = T_e = T_G$ than observed in the experiments. This trend is similar to that observed in previous comparisons, e.g., for the molecule CF_3Br [20]. The differences may be – at least in part – due to the fact that other vibrational modes, not taken into account in the theoretical model, may play a role and lead to a stronger dependence on the vibrational temperature.

5. Conclusions

Results from a joint experimental study of electron attachment to chloroform ($CHCl_3$) molecules in the gas phase are reported. In an electron swarm study involving a pulsed Townsend technique with equal gas and electron temperatures, accurate attachment rate coefficients were determined over the temperature range 295–373 K; they show an Arrhenius-type rise with increasing temperature, corresponding to an activation energy of 0.11(1) eV. In a high resolution electron beam experiment involving two versions of the laser photoelectron attachment method, the relative cross section for Cl^- formation from $CHCl_3$ over the energy range 0.001–1.25 eV at the gas temperature T_G = 300 K was measured. With reference to our thermal attachment rate coefficient $k(T = 300\,K) = 3.9(2) \times 10^{-9}$ cm^3 s^{-1}, a new highly resolved absolute attachment cross section for T_G = 300 K was determined. This cross section is extended to higher energies by measurements carried out with the TEM-TOF apparatus at Belfast which also provided new cross sections for the distinctly weaker fragment anions CCl_2^- and HCl_2^-. The resulting total absolute cross section for anion formation is used to calculate the dependence of the attachment rate coefficient $k(T_e;T_G)$ on electron temperature T_e over the range 50–15000 K at the fixed gas temperature T_G = 300 K. In addition, we report the dependence of the relative cross section for Cl^- formation on gas temperature (T_G = 310–435 K).

For comparison with the experimental data, R-matrix calculations have been carried out for the DEA cross section of the dominant anion channel Cl^-. The results predict the dependence of the DEA cross section on the initial vibrational level ν_3^i and provide a good description of the main experimental observations.

Acknowledgments

The authors acknowledge the stimulation provided for this joint project through the ESF network EIPAM (*Electron-Induced Processing at the Molecular level*). The research in Siedlce was supported from scientific funds for the years 2005–2008 under Grant 3 T09A 111 29. KG would like to thank the European Social Fund for providing a PhD studentship. TAF, KG and LMG would like to thank the EPSRC for their support of this work through grant EP/F031025/1. The studies in Innsbruck have been supported by the FWF, Vienna, Austria and the European Commission, Brussels. S. Denifl acknowledges an Apart-fellowship from the Austrian Academy of Sciences. IIF was supported by the US National Science Foundation, Grant PHY-0652866. The work in Kaiserslautern was supported by the Deutsche Forschungsgemeinschaft (HO 427/29) and by the Forschungszentrum OTLAP. We thank P. D. Burrow for providing his total cross section for DEA to $CHCl_3$ in numerical form.

References

[1] L.G. Christophorou (Ed.), Electron-Molecule Interactions and Their Applications, vols. 1 and 2, Academic Press, New York, 1984.
[2] A. Chutjian, A. Garscadden, J.M. Wadehra, Phys. Rep. 264 (1996) 393.
[3] L.G. Christophorou, J.K. Olthoff, Fundamental Electron Interactions with Plasma Processing Gases, Kluwer Academic/Plenum Publ, New York, 2004.
[4] E. Illenberger, in: C.-Y. Ng (Ed.), Photoionization and Photodetachment Part II, Adv. Ser. Phys. Chem., vol. 10B, World Scientific, Singapore, 2000, p. 1063.
[5] H. Hotop, M.-W. Ruf, M. Allan, I.I. Fabrikant, Adv. At. Mol. Opt. Phys. 49 (2003) 85.
[6] D. Klar, M.-W. Ruf, H. Hotop, Aust. J. Phys. 45 (1992) 263.

[7] L.G. Christophorou, J.K. Olthoff, J. Phys. Chem. Ref. Data 29 (2000) 267.
[8] Y. Liu, L. Suess, F.B. Dunning, J. Chem. Phys. 122 (2005) 214313.
[9] K. Aflatooni, P.D. Burrow, J. Chem. Phys. 113 (2000) 1455.
[10] A. Modelli, Trends Chem. Phys. 6 (1997) 57.
[11] G.A. Gallup, K. Alfatooni, P.D. Burrow, J. Chem. Phys. 118 (2003) 2562.
[12] P.D. Burrow, A. Modelli, N.S. Chiu, K.D. Jordan, J. Chem. Phys. 77 (1982) 2699.
[13] M. Guerra, D. Jones, G. Distefano, F. Scagnolari, A. Modelli, J. Chem. Phys. 94 (1991) 484.
[14] K. Aflatooni, G.A. Gallup, P.D. Burrow, J. Phys. Chem. A 104 (2000) 7359.
[15] O.J. Orient, A. Chutjian, R.W. Crompton, B. Cheung, Phys. Rev. A 39 (1989) 4494.
[16] L.G. Christophorou, Z. Phys. Chem. 196 (1996) 195.
[17] T. Andersen, H.K. Haugen, H. Hotop, J. Phys. Chem. Ref. Data 28 (1999) 1511.
[18] David R. Lide (Editor-in-Chief), CRC Handbook of Chemistry and Physics, 88th Edition, CRC Press, Taylor&Francis Group, Boca Raton, FL, USA (2008).
[19] R.S. Wilde, G.A. Gallup, I.I. Fabrikant, J. Phys. B 33 (2000) 5479.
[20] S. Marienfeld, T. Sunagawa, I.I. Fabrikant, M. Braun, M.-W. Ruf, H. Hotop, J. Chem. Phys. 124 (2006) 154316.
[21] I.I. Fabrikant, H. Hotop, J. Chem. Phys. 128 (2008) 124308.
[22] D. Smith, P. Spaněl, Adv. Atom. Molec. Opt. Phys. 32 (1994) 307.
[23] T. Sunagawa, H. Shimamori, Int. J. Mass Spectrom. 205 (2001) 285.
[24] M. Braun, I.I. Fabrikant, M.-W. Ruf, H. Hotop, J. Phys. B 40 (2007) 659.
[25] T.G. Lee, J. Phys. Chem. 67 (1963) 360.
[26] R.P. Blaunstein, L.G. Christophorou, J. Chem. Phys. 49 (1968) 1526.
[27] W.E. Wentworth, R. George, H. Keith, J. Chem. Phys. 51 (1969) 1791.
[28] J.M. Warman, M.C. Sauer, Int. J. Radiat. Phys. Chem. 3 (1971) 273.
[29] A.A. Christodoulides, L.G. Christophorou, J. Chem. Phys. 54 (1971) 4691.
[30] E. Schultes, A.A. Christodoulides, R.N. Schindler, Chem. Phys. 8 (1975) 354.
[31] A.A. Christodoulides, R. Schumacher, R.N. Schindler, Z. Naturforsch. 30a (1975) 811.
[32] J.A. Ayala, W.E. Wentworth, E.C.M. Chen, J. Phys. Chem. 85 (1981) 3989.
[33] D. Smith, N.G. Adams, E. Alge, J. Phys. B 17 (1984) 461.
[34] C.J. Marotta, C. Tsai, D.L. McFadden, J. Chem. Phys. 91 (1989) 2194.
[35] H. Shimamori, Y. Tatsumi, Y. Ogawa, T. Sunagawa, J. Chem. Phys. 97 (1992) 6335.
[36] P. Spaněl, S. Matejcik, D. Smith, J. Phys. B: At. Mol. Opt. Phys. 28 (1995) 2941.
[37] S.J. Burns, J.M. Matthews, D.L. McFadden, J. Phys. Chem. 100 (1996) 19436.
[38] P. Spaněl, D. Smith, Czech. J. Phys. 48 (1998) 1119.
[39] F.H. Dorman, J. Chem. Phys. 44 (1966) 3856.
[40] D. Spence, G.J. Schulz, J. Chem. Phys. 63 (1973) 1800.
[41] J.P. Johnson, L.G. Christophorou, J.G. Carter, J. Chem. Phys. 67 (1977) 2196.
[42] H.-U. Scheunemann, E. Illenberger, H. Baumgärtel, Ber. Bunsenges. Phys. Chem. 84 (1980) 580.
[43] S.C. Chu, P.D. Burrow, Chem. Phys. Lett. 172 (1990) 17.
[44] S. Matejcik, G. Senn, P. Scheier, A. Kiendler, A. Stamatovic, T.D. Märk, J. Chem. Phys. 107 (1997) 8955.
[45] S. Matejcik, V. Foltin, M. Stano, J.D. Skalny, Int. J. Mass. Spectrom. 223-224 (2003) 9.
[46] S. Denifl, A. Mauracher, P. Sulzer, A. Bacher, T.D. Märk, P. Scheier, Int. J. Mass Spectrom. 265 (2007) 139.
[47] P. Spanel, D. Smith, Int. J. Mass Spectrom. Ion Proc. 129 (1993) 193.
[48] A. Kalamarides, R.W. Marawar, M.A. Durham, B.G. Lindsay, K.A. Smith, F.B. Dunning, J. Chem. Phys. 93 (1990) 4043.
[49] Y. Wang, L.G. Christophorou, J.K. Verbrugge, J. Chem. Phys. 109 (1998) 8304.
[50] J. deUrquijo, C.A. Arriaga, C. Cisneros, I. Alvarez, J. Phys. D: Appl. Phys. 32 (1999) 41.
[51] J. Kopyra, J. Wnorowska, M. Foryś, I. Szamrej, Int. J. Mass Spectrom. 268 (2007) 60.
[52] I. Szamrej, M. Foryś, Radiat. Phys. Chem. 33 (1989) 393.
[53] T.A. Field, A.E. Slattery, D.J. Adams, D.D. Morrison, J. Phys. B 38 (2005) 255.
[54] S. Denifl, S. Ptasinska, M. Probst, J. Hrusak, P. Scheier, T.D. Märk, J. Phys. Chem. A 108 (2004) 6562.
[55] D. Klar, M.-W. Ruf, H. Hotop, Meas. Sci. Technol. 5 (1994) 1248.
[56] J.M. Weber, E. Leber, M.-W. Ruf, H. Hotop, Eur. Phys. J. D 7 (1999) 587.
[57] M. Braun, S. Barsotti, S. Marienfeld, E. Leber, J.M. Weber, M.-W. Ruf, H. Hotop, Eur. Phys. J. D 35 (2005) 177.
[58] D. Klar, M.-W. Ruf, H. Hotop, Int. J. Mass Spectrom. 205 (2001) 93.
[59] I.I. Fabrikant, Phys. Rev. A 43 (1991) 3478.
[60] I.I. Fabrikant, H. Hotop, M. Allan, Phys. Rev. A 71 (2005) 022712.
[61] K. Irikura, private communication, R.D. Johnson III, http://srdata.nist.gov/cccbdb/.
[62] T. Shimanouchi, Tables of Molecular Vibrational Frequencies, Vol. I, Nat. Stand. Ref. Data Ser. 39 (1972) 54.
[63] A.M. Lane, R.G. Thomas, Rev. Mod. Phys. 30 (1958) 257.
[64] S.A. Kalin, A.K. Kazansky, J. Phys. B 23 (1990) 4377.
[65] S. Marienfeld, I.I. Fabrikant, M. Braun, M.-W. Ruf, H. Hotop, J. Phys. B 39 (2006) 105.
[66] I.I. Fabrikant, H. Hotop, Phys. Rev. A 63 (2001) 022706.
[67] A. Schramm, I. I: Fabrikant, J.M. Weber, E. Leber, M.-W. Ruf, H. Hotop, J. Phys. B 32 (1999) 2153.
[68] A. Schramm, M.-W. Ruf, M. Stano, S. Matejcik, I.I. Fabrikant, H. Hotop, J. Phys. B 35 (2002) 4179.
[69] P. Cicman, J.D. Skalny, J. Fedor, N.J. Mason, P. Scheier, E. Illenberger, T.D. Märk, Int. J. Mass Spectrom. 260 (2007) 85.